

bradscholars

Nanoscale ZrRGOCuFe layered double hydroxide composites for enhanced photocatalytic degradation of dye contaminant

Item Type	Article
Authors	Kumar, O.P.;Ashiq, M.N.;Shah, S.S.A.;Akhtar, S.;Mudhar, M.A.;Mujtaba, Iqbal;Rehman, A. ur
Citation	Kumar OP, Ashiq MN, Shah SSA et al (2021) Nanoscale ZrRGOCuFe layered double hydroxide composites for enhanced photocatalytic degradation of dye contaminant. Materials Science in Semiconductor Processing. 128: 105748.
DOI	https://doi.org/10.1016/j.mssp.2021.105748
Rights	© 2021 Elsevier. Reproduced in accordance with the publisher's self-archiving policy. This manuscript version is made available under the CC-BY-NC-ND 4.0 license (http://creativecommons.org/licenses/by-nc-nd/4.0/)
Download date	2026-03-09 18:44:16
Link to Item	http://hdl.handle.net/10454/18902

Nanoscale ZrRGOCuFe layered double hydroxide composites for enhanced photocatalytic degradation of dye contaminant

Ome Parkash Kumar ^a, Muhammad Naeem Ashiq ^b, Syed Shoaib Ahmad Shah ^c, Shahbaz Akhtar ^d, Aziz ur Rehman ^e, Mudhar A. Al. Obaidi ^f and Iqbal M. Mujtaba ^g

^{a,c,f} Department of Chemistry, The Islamia University of Bahawalpur, Bahawalpur 63100, Pakistan

^b Institute of Chemistry Bahaudin Zikrya University Multan, Multan

^d Department of Biochemistry and Biotechnology, The Islamia University of Bahawalpur, Bahawalpur 63100, Pakistan

^f Middle Technical University, Technical Institute of Baquba, Baquba, Dayala – Iraq

^g Chemical Engineering Department, Faculty of Engineering and Informatics. The University of Bradford. Bradford, West Yorkshire BD7 1DP, UK

*Corresponding author, Tel.: +92 333 6133770

E-mail address: azizypk@yahoo.com

Abstract

Co-precipitation method was used to prepare non-stoichiometric pristine copper and iron layered double hydroxide (LDH) doped with zirconium and embedded with reduced graphene oxide. The composite materials (ZrRGOCuFe LDHs) were studied for the photodegradation of methylene blue (MB) dye as a model contaminant from an aqueous solution. These composites were fully characterized by X-rays diffraction (XRD), Scanning electron microscopy (SEM), Energy Dispersive X-ray Spectroscopy (EDX), Fourier transform infrared spectroscopy (FTIR), photoluminescence (PL), Raman spectroscopy and Electrochemical Impedance Spectroscopy (EIS). The results of Raman, Photoluminescence and Electrochemical Impedance Spectroscopy revealed the presence of oxygen defects level in the composites. Such defects are believed to be essential for boosting the catalytic potential of the composites. The secondary pollution manifested by transition metal ions is usually tackled by inducing heterogeneous catalysis. Herein, pristine CuFe LDH has been doped with Zr and RGO moieties to realize heterogeneous catalysis within ZrRGOCuFe LDH dopants. An admirable band ranging between 1.74-2.0 eV

30 was obtained for the doped materials. The remarkable photodegradation efficiency of 95.2% was
31 achieved by using heterogeneous photocatalyst $Zr_{0.6}RGOCuFe$ LDH within 75 minutes by using
32 1.0 g/L of the photocatalyst for the degradation of methylene blue dye solution of 10 ppm at pH
33 7.0 under visible light irradiation. The total organic content (TOC) analysis has revealed removal
34 of 92% organic content from an sstability and reusability capacity of the catalyst even after three
35 successive cycles. The reaction kinetics and proposed photocatalytic mechanism were also
36 explained in detail.

37 **Keywords:** Co-precipitation; Dye degradation; Heterogeneous catalysis; Methylene blue; LDHs;
38 $ZrRGOCuFe$ LDH

39 **1. Introduction**

40 The tremendous use of dyes in plastic, rubber, food, cosmetics, textile, carpet, leather, paint,
41 printing, photo electrochemical cell and the paper industries has raised the production of dye
42 wastewater [1-5].The majority of the synthetic dyes are non-biodegradable, however upon
43 mixing in water impart intense colour.The coloured water results in the permeation of light
44 which may endanger living organisms in water bodies [6]. Methylene blue (MB) a cationic dye is
45 being used mostly in dyeing of cotton, silk and wood. However, its direct disposal poses potential
46 danger to the environment and disturbs the balance of the ecosystem [7-9].Thus, discharges
47 containing significant amount of methylene blue dye are required to be treated prior to their
48 disposal into the water bodies. Various methods have been employed for the extraction of
49 methylene blue dye from the effluent water, physical, chemical and biological modes involving
50 biodegradation,noxidation, reverse-osmosis, adsorption, photodegradation, ion exchange,
51 coagulation and evaporation [10-13]. Among these, photodegradation is regarded as the superior
52 method because it has power to oxidize the concerned pollutant completely within short period

53 of time. Layered double hydroxide (LDH) is an emerging class of cationic clays widely used as
54 a photocatalyst or the photocatalyst carrier owing to their nontoxicity and the superior
55 adsorption ability [14]. These are synthetic as well as occur abundantly in nature and represented
56 with general formula of $[M^{2+}_{1-x}M^{3+}_x(OH)_2]^{x+1}(A^{n-})_{x/n} \cdot yH_2O$. Where, M^{II} and M^{III} represent
57 metal cations which are octahedrally bonded to the OH^- in the brucite-like sheets [15-17]. In
58 formula M^{2+} / M^{3+} ratio could be greater than two, may comprise of divalent (Mg^{2+} , Cu^{2+}) and
59 trivalent (Fe^{3+} , Al^{3+}) metal cations [18]. LDHs as a whole bears positive charge but additional
60 anions (CO_3^{2-} , NO_3^{-1}) along with H_2O molecules are located in the interlayer to stabilize the
61 charge imbalance [19]. The orientation and size of anions and the hydrates determine the
62 interlayer of the LDH. LDHs and their derivatives have been used as heterogeneous catalysts
63 [20]. These are being explored for tackling environmental problems such as removal of
64 polychlorinated biphenyls, phenols, nitrates and carbon dioxide. Numerous other applications
65 have also been reported regarding energy fuels and super capacitor [21-23]. General methods for
66 the preparation of LDHs include sol-gel, co-precipitation, hydrothermal and pulsed laser ablation
67 [24-27]. As LDHs possess low band gap energy, these could easily be excited by the exposure of
68 UV-visible radiation thus making feasible water reduction and photocatalytic degradation. It has
69 been discovered that the introduction of a heterojunction within a compound may act as the co-
70 catalyst for the separation of photo-excitation [28]. Furthermore, the doping of Zr with graphen
71 embedded CuFe LDH causes rapid charge transfer due to synergic effect created by zirconium
72 and reduced graphene oxide [29, 30]. In this research, pristine CuFe LDH and its derivative
73 heterogeneous ZrRGOCuFe LDHs were explored for the enhanced degradation of methylene
74 blue dye. The composites ZrRGOCuFe LDHs are found more effective with respect to the
75 degradation of MB than earlier cited CuFe LDHs and its derivatives. Those may require H_2O_2 ,

76 UV radiations or persulphate for effective photodegradation [31-33]. While, ZrRGOCuFe LDHs
77 demonstrates enhanced photodegradation of MB under the visible light irradiation.

78 **2. Experimental section**

79 **2.1. Chemicals**

80 Copper nitrate trihydrate (99%), sodium hydroxide (95%), sodium carbonate (99.9%), KOH
81 (99%), ethanol (99.5%), KMnO_4 ($\geq 99\%$), calcium chloride (99%) were obtained from Merck,
82 ferric nitrate nonahydrate (99.5%) received from bio-WORLD, while, Zirconium nitrate
83 pentahydrate (99.5%), NaBH_4 (99%) and hydrogen peroxide (30%) were purchased from Sigma-
84 Aldrich. Graphite powder (99.99%) and phosphoric acid (85%) were supplied by BDH
85 chemicals Ltd. Throughout, deionized water was used.

86 **2.2. Synthesis of graphene oxide**

87 Graphene oxide (GO) was synthesized by the treatment of graphite powder by modified
88 hummers method [34]. Briefly, 122 ml of concentrated sulphuric acid and 14 ml of phosphoric
89 acid were mixed and stirred for 20 minutes. Then, added 1.0 g of graphite powder in the mixture
90 of acids with continuous stirring mode. After that, 6.0 g of KMnO_4 powder was slowly added
91 into the above mentioned mixture and stirred vigorously for six hours. For the removal of excess
92 of KMnO_4 , 3.0 ml of hydrogen peroxide was added drop wise and stirred for 15 minutes. The
93 suspension was allowed to cool at the room temperature. Next, 50 ml of HCl (2M) solution and
94 140 ml of water were added and stirring continued for 20 minutes. Afterwards, the suspension
95 was centrifuged for 15 minutes at 6000 rpm. The residue was collected and washed with HCl and
96 water and dried in a vacuum oven at 60 °C for 24 hours.

97 **2.3. Synthesis of reduced graphene oxide**

98 For the preparation of Reduced Graphene Oxide (RGO), typically 0.5 g of graphene oxide was
99 added in 100 ml of deionized water. Next, 1.15 g of sodium borohydride was dissolved in 15 ml
100 cold water was slowly added in the mixture. Then, 0.90 g of calcium chloride was added into as
101 prepared mixture and aged at room temperature for 24 hours. Furthermore, the suspension was
102 washed with water to maintain pH 6. Next, 5.0 g of ascorbic was added into the above
103 suspension and stirred for 30 minutes, the color of suspension changed to dark black. Finally, it
104 was washed and centrifuged to get RGO. Thus, obtained product was dried at 80 °C for six hours
105 in the vacuum oven [35].

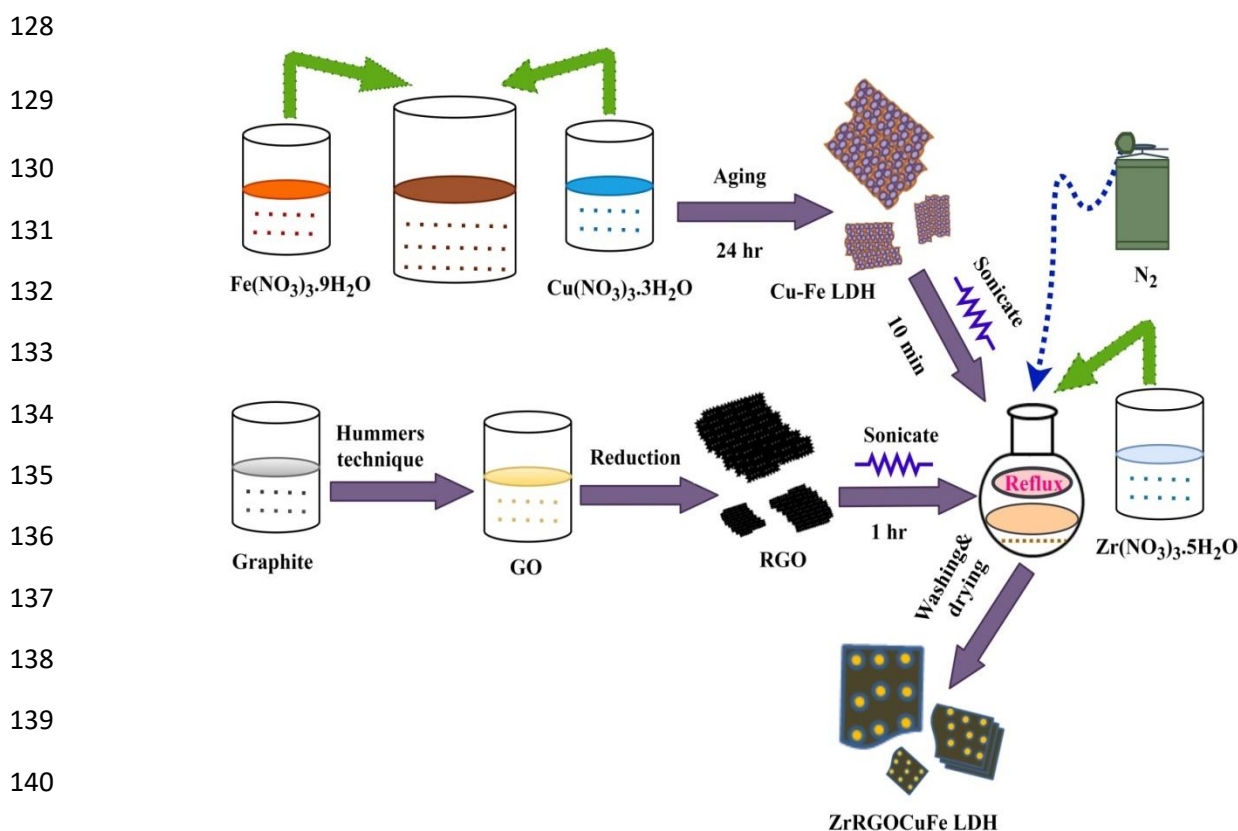
106 ***2.4. Synthesis of CuFe LDH***

107 In a typical procedure, CuFe LDH was prepared by mixing 2.41g (0.01M) of copper nitrate
108 trihydrate and 4.84g (0.012M) of iron nitrate nonahydrate in 100 ml of deionized water, the
109 overall mole ratio of M^{2+}/M^{3+} was maintained at 0.83. The pH of the solution was adjusted at 9.0
110 by addition of 1.0 M sodium hydroxide and 0.01M sodium carbonate solution. Then, it was aged
111 for 24 hours at room temperature. Further, the suspension was filtered and washed with
112 deionized water and ethanol. The resulting product was heated at 80 °C for 12 hours in the oven.

113 ***2.5. Formation of ZrRGOCuFe LDHs composite***

114 Heterogeneous ZrRGOCuFe LDH composites were prepared by co-precipitation method.
115 Typically, 0.15g of pristine reduced graphene oxide was added into 50 ml of ethanol and then
116 sonicated for 60 min for homogenization. Afterwards, suspension was transferred to three necked
117 500 ml flask and denoted by the component A. Further, 1.6g of as- synthesized CuFe LDH was
118 dissolved into 50 ml of deionized water and sonicated this was recognized as the component B.
119 Furthermore, added the component B into the component A and this was termed as the
120 component C. The Changing amounts of zirconium nitrate pentahydrated solution ($x= 0.004$ and

121 0.006 M) were also added to the above mixture. The pH of the solution was adjusted to 8.5 by
 122 addition of 1.0 M KOH solution drop wise. The reaction was carried out under the protection
 123 nitrogen for first two hours to check the formation of excessive amount of corresponding metal
 124 oxides. As a whole solution mixture was refluxed for 6 hours at the temperature of 60°C. Then,
 125 the product was collected by centrifugation and washing with ethanol and water thrice. Finally,
 126 the product was heated in the oven for 6 hours at 110 °C and the product was crushed into the
 127 powder for further use.



141 **Fig. 1.** Schematic portrayal for the formation of ZrRGO CuFe layered double hydroxide composites
 142 The product was denoted as Zr_{0.4}RGO CuFe LDH and Zr_{0.6}RGO CuFe LDH. The schematic
 143 portrayal for the formation of ZrRGO CuFe layered double hydroxides nanocomposite has been
 144 demonstrated in the Fig. 1.

145 **2.5. Characterization methods of catalysts**

146 The X-Rays Diffraction (XRD) pattern of precursor and products were obtained by using Bruker
147 D8 Advanced Powder X-rays diffractometer in $2\theta^\circ$ range $10-70^\circ$ (Cu $K\alpha$ radiation, $\lambda=1.54178$
148 Å). The morphology of the materials was revealed by Scanning Electron Microscopy (SEM,
149 TESCAN MIRA3 LMU) at applied voltage was 20 KV. The absorbance properties of samples
150 were carried out using CeCil CE 7400 UV-Visible spectrophotometer. The electrochemical
151 properties were determined at the room temperature by the use of Autolab PGSTAT12 (three
152 electrodes system). Photoluminescence (PL) spectrum was performed by Cary Eclipse (MY
153 18060003) fluorescence spectrophotometer while FTIR spectrum was measured in Tensor
154 Bruker (Germany). A Raman spectrum of samples was measured by using Raman spectrometer
155 (Lab RAM, HR800) with a He-Ne laser source (633nm) as an excitation source. A multi N/C UV
156 HS TOC Analyzer from Analytik Jena was further used to investigate photomineralization of the
157 methylene blue dye.

158 ***2.6. Evaluation of catalytic activity with ZrRGOCuFe LDHs composites***

159 The degradation of methylene blue (MB) dye was carried out in a 100 cm^3 glass beaker. To
160 evaluate photodegradation of MB with ZrRGOCuFe LDHs, blank experiment was conducted
161 without addition of the photocatalyst. No significant photodegradation was noticed on exposing
162 the solution to the visible light radiation. This indicated that methylene blue dye is very stable in
163 aqueous medium under visible light in the absence of ZrRGOCuFe LDHs. The dye solution of
164 20 ml having 10 and 40 ppm concentration at different pH values was separately mixed into 0.02
165 of the photocatalyst. Afterwards, the suspension was kept into the dark for 30 minutes for the
166 adsorption and desorption equilibrium process to take place under continuous magnetically
167 stirring conditions. It was irradiated with 200 watts ordinary light tungsten bulb for certain time
168 duration. The distance between the radiation source and the suspension was adjusted to 15

169 centimeters. Further, the solution was centrifuged at 6000 rpm for 13 minutes, filtered and finally
170 analyzed for the determination of the degradation. The photodegradation was calculated by using
171 equation (1) [36].

$$172 \quad \% \text{ degradation of methylene blue dye} = \frac{C_0 - C}{C} \times 100 \quad (1)$$

173 Where, C_0 the initial concentration of the dye and C is the final concentration of the dye.

174 **3. Results and discussion**

175 The UV-visible spectra of the samples were taken to find their optical properties. Variation in
176 band edges were observed, further band gap energy was calculated using equation (2) [37].

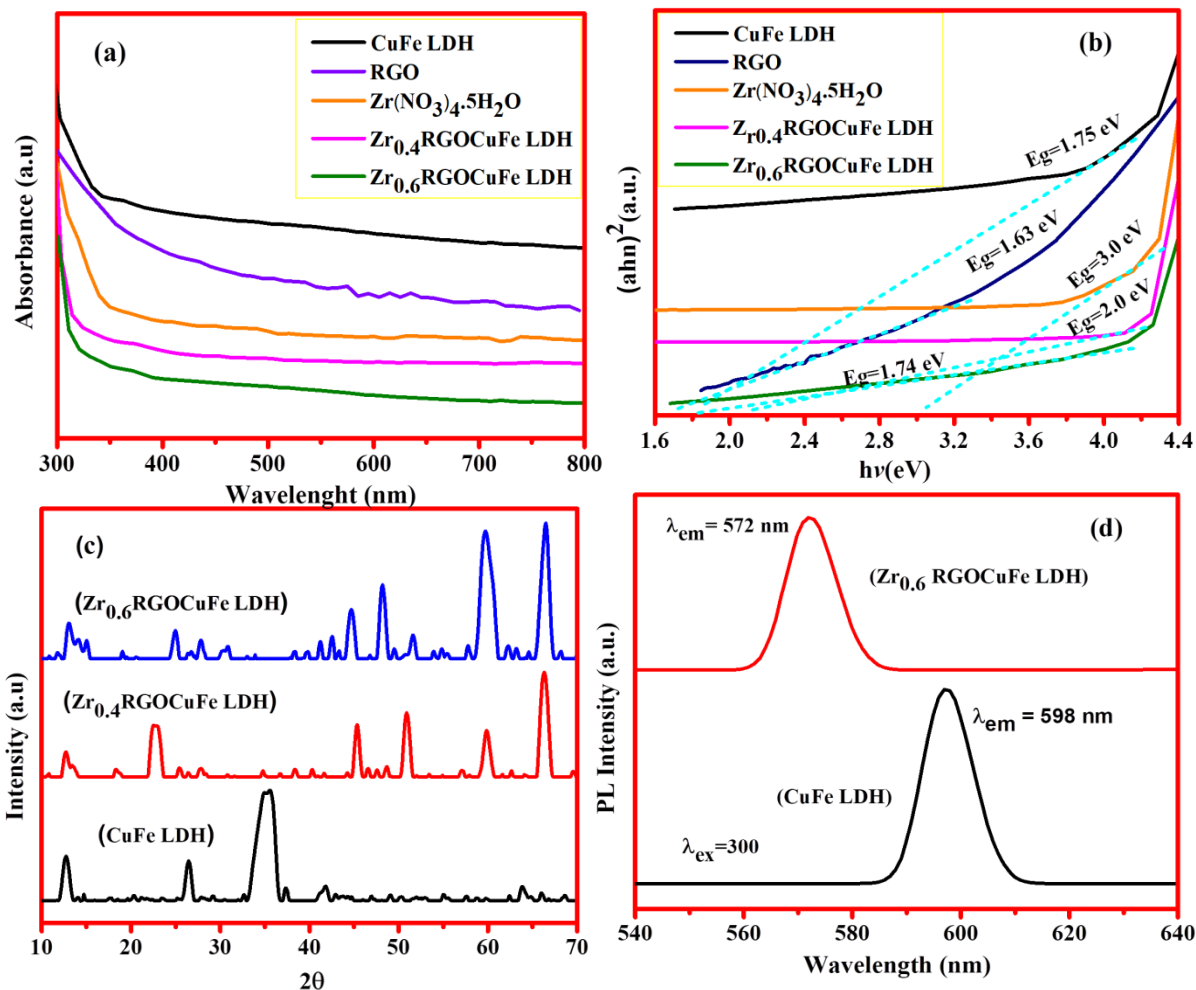
$$177 \quad (ah\nu) = A (h\nu - E_g)^n / h\nu \quad (2)$$

178
179 Where, a = coefficient of absorption and A = independent energy constant h = Planck's constant
180 ν = light $n=2$ is case of direct transition and E_g = band gap energy, respectively. Fig. 2a and b
181 describe the UV-Visible and band gaps of precursors and the doped materials. The band of
182 zirconium nitrate pentahydrate and reduced graphene oxide (RGO) was calculated as 3.0 eV and
183 1.51 eV. The band gap of the precursor CuFe LDH was calculated as 1.75 eV. The bands gaps of
184 doped samples $Zr_{0.4}RGO$ CuFe LDH and $Zr_{0.6}RGO$ CuFe LDH were estimated as 2.0 and 1.74
185 eV, respectively. The decreasing trend of band gap energy in the doped samples was attributed to
186 increase in the zirconium content which may narrow down the valence band. All the band gaps
187 of the precursors and doped materials lie in the visible absorption region.

188 X-rays diffraction spectroscopy was employed for the determination of crystal structure and
189 lattice parameters [38]. The CuFe LDH exhibits XRD reflections at $2\theta = 12.8^\circ, 25.6^\circ, 35.55^\circ,$
190 41.91° and 49.23° which corresponded to the standard reflections of (JCPDS 41-1428) [39-41]. In

191 the composite ZrRGOcCuFe LDH, the presence of two peaks at $2\theta = 25^\circ, 30^\circ$ was ascribed to
 192 reduced graphene oxide and ZrO_2 , respectively. The X-RD patterns of the dopants and precursors
 193 have been described in Fig. 2(c). The average crystallite size was determined by applying
 194 Debye-Scherer formula with respect to most intense peak observed in the pristine CuFe LDH
 195 [42].

$$D = \frac{k\lambda}{\beta \cos\theta}$$



211 **Fig. 2.** (a) Absorbance (b) Tauc plot of compounds of precursors and composite (c) XRD patterns of pristine CuFe
 212 LDH and composites (d) PL spectra of CuFe LDH and composite

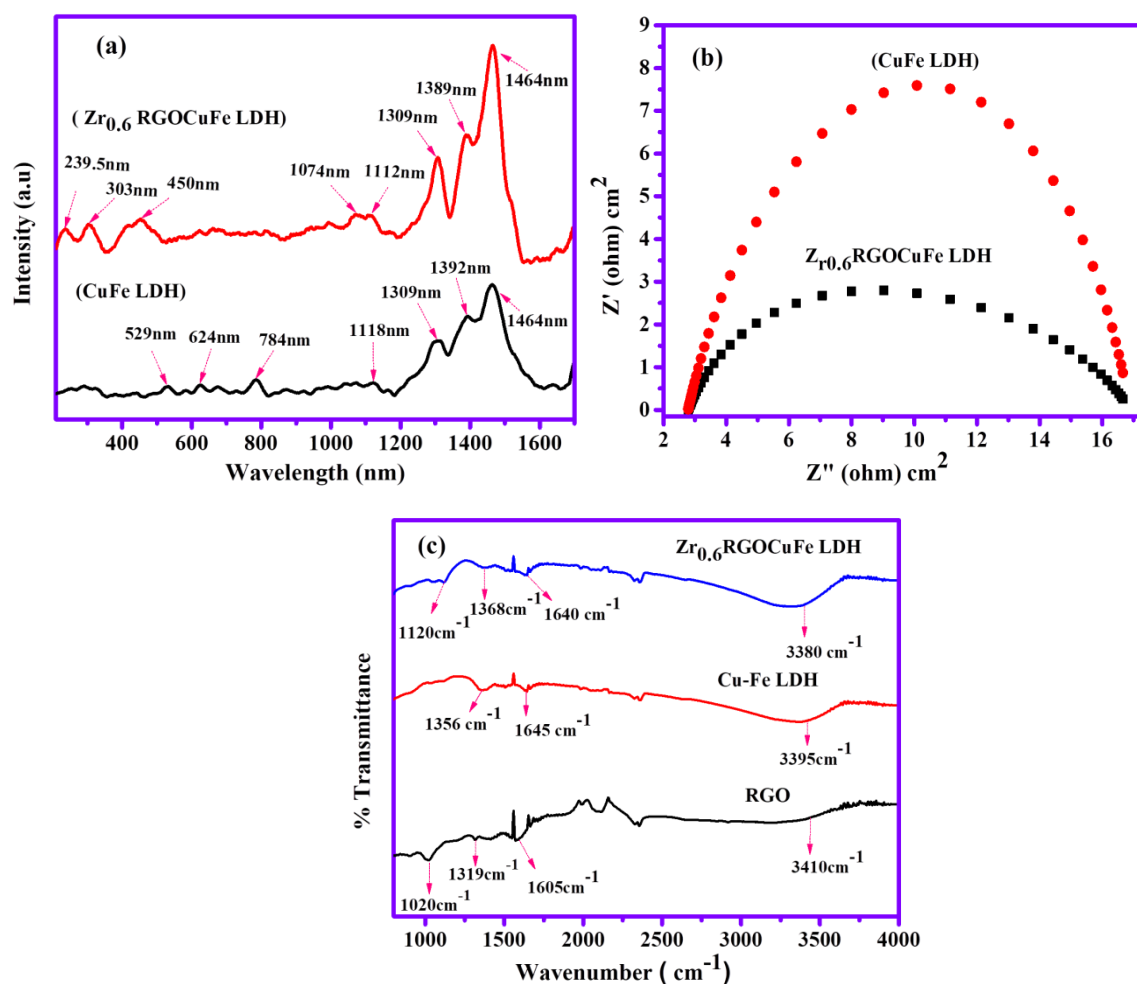
213 The average crystallite size, k is the crystallite shape factor, $\lambda = 1.540$ nm wave length of Cu K α
214 wavelength, β is the width of diffraction peak and θ Bragg's angle. The average crystallite size
215 was found 17.43 nm for CuFe LDH. While in sample Fig. 2(c) the most intense peaks are
216 observed at $2\theta = 66.30^\circ$ and 66.40° so the calculated average crystallite size is 19.83 and 19.84
217 nm, respectively.

218 Along with providing insight into defect state of semiconductors, photoluminescent properties
219 explained the effect of impurities on defect state. A single excitation wave length of 300 nm was
220 employed at room temperature (25°C) to obtain photo luminescent spectra CuFe LDH and
221 Zr_{0.6}RGOCuFe LDH showed distinct emission spectra visible region at wavelengths of 597 and
222 572 nm, respectively as depicted in Fig. 2(d). These emissions could be ascribed to the presence
223 of oxygen vacancy defects ($\text{VO}\cdot$) in the ZrRGOCuFe LDHs [43]. The photoluminescence
224 spectroscopy revealed the charge separation in as-synthesized material ZrRGOCuFe LDHs,
225 which provides onus for superior photocatalytic activities.

226 Fig. 3(a) explains the Raman spectra for the pristine CuFe LDH and dopant and nanocomposite
227 Zr_{0.6}RGOCuFe LDH. Raman spectroscopy is very highly sensitive and non-destructive technique
228 used to find phase transition, bond vibration and the occurrence of oxygen defects in the
229 composites. Seven peaks were identified in the pure compound, five at the frequency of 529,
230 624, 784, 1118, and 1309, 1392 and 1464 cm^{-1} . In case of dopant, two peaks were observed at
231 239.5, 303, 450, 1074, 1112, 1309, 1464 cm^{-1} . The peak appearing at 529 cm^{-1} was ascribed to
232 brucite like structure of layered double hydroxide.

233 The distortion in the region of 529-620 cm^{-1} was assigned to the stretching symmetry of the M-O
234 ($\text{Fe}^{3+}/\text{Cu}^{2+}$ or Cu^{1+}) bond in the CuFe LDH. A weak single peak centered at 784 cm^{-1} was
235 designated to the presence of M-O bond in the pristine LDH. However, remaining three stronger

236 spectra at 1309, 1392 and 1464 cm^{-1} related to the symmetrical stretching and translational
 237 vibration modes of intercalated CO_3^{2-} anions [44, 45].
 238 Electrochemical Impedance Spectroscopy (EIS) was also carried out to investigate charge
 239 transfer process between electrolyte and electrode interfaces. Fig. 3(b) exhibited EIS spectra of
 240 CuFe LDH and $\text{Zr}_{0.6}\text{RGO/CuFe LDH}$. The smaller arc diameter in the Nyquist plots indicated the
 241 presence of smaller charge resistance and faster electronic transport in the ZrRGO/CuFe LDHs
 242 [46]. As a result of low resistant and accelerated charge transfer ZrRGO/CuFe LDHs
 243 demonstrated an efficient catalytic activity.

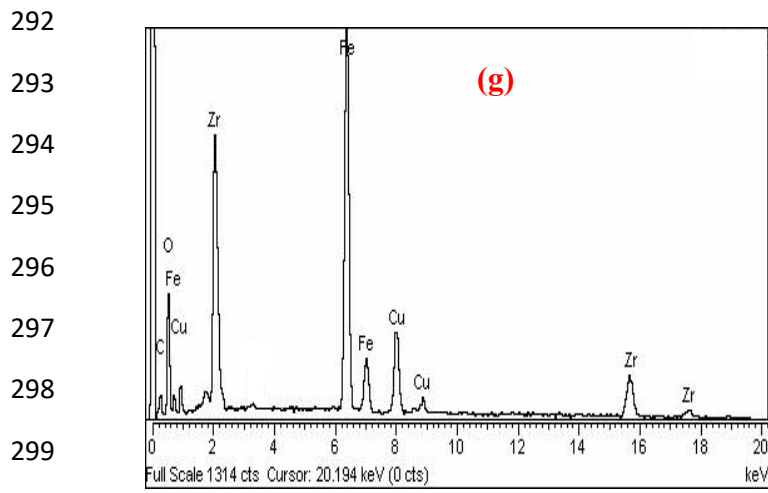
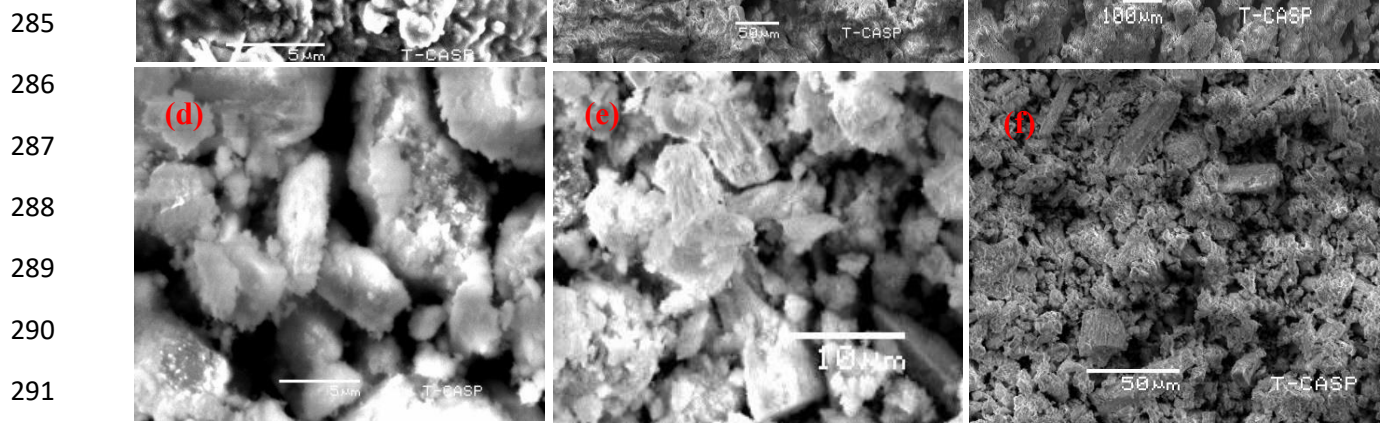


261 **Fig.3.** (a) Raman spectrum of the precursor CuFe LDH and ZrRGO/CuFe LDHs composite (b) EIS Nyquist plot of
262 precursor and composite (c) FTIR spectra of precursors and composite

263
264 Fourier Transform Spectroscopy (FTIR) provides information about the presence of functional
265 groups in the materials. In Fig. 3(c) the peaks appearing at 1020, 1319, 1605, 2360 and 3410 cm^{-1}
266 were ascribed to the presence of RGO. The layered hydroxide CuFe exhibited peaks at 1356,
267 1645, 2362 and 3395 cm^{-1} , while composite ZrRGO/CuFe LDH material showed peaks at 1120,
268 1368, 1640, 2364 and 3380 cm^{-1} . The peaks in the range of 1120 and 1645 cm^{-1} were attributed
269 to C=O and C-N vibrations, while a prominent peak at 1356 cm^{-1} in CuFe LDH was
270 corresponded to vibrations of CO_3^{2-} interlayer anions. However, the broad absorption peaks
271 ranging from 3380 to 3410 cm^{-1} were assigned to O-H stretching vibrations layered hydroxides
272 [47, 48].

273 Scanning Electron Microscopic (SEM) and Energy Dispersive X-ray (EDX) microanalysis of
274 ZrRGO/CuFe LDHs composite are presented in Fig.4(a-e). The SEM images of CuFe LDH
275 exhibit layered structure with small pores, overall it seems similar to honey comb. On the other
276 hand, ZrRGO/CuFe LDH appear like rod, some particle also exist in irregular shapes particles.
277 The samples ZrRGO/CuFe LDHs composite were analyzed using a primary beam voltage of 20
278 KV. The blends of CuFe LDH with RGO and Zr afforded the composite material that revealed
279 layered structure with deposition of Zr on the top in the form of irregular patches. These may be
280 due to immature doping of the composite.

281 Energy Dispersive X-ray microanalysis of ZrRGO/CuFe LDH (Fig.4g) composite has exhibited
282 the presence of Cu, Fe, O, C and Zr. The stoichiometric ratios of the precursors in the EDX
283 micrograph demonstrated a successful synthesis of the composite. EDX is the surface analysis
284 technique used for the comparison of elements in the given material.



Element	Weight%	Atom%
CK	10.25	27.04
OK	20.01	39.62
FeK	35.42	35.42
CuK	8.14	4.17
ZrL	26.18	9.99
Total	100	

300

301

302

303

304

305

306

307

308 **Fig. 4.** SEM images (a-c) CuFe LDH (d-f) SEM images of ZrRGOCuFe LDHs (g) EDX micrograph of ZrRGOCuFe LDHs
 309 composite.

310 **3.1 Photocatalytic dye degradation studies**

311 The photocatalytic activity of MB dye was carried out under the same experimental conditions to
 312 assess the influence of visible light. The visible light is believed to photosensitize the dye. The

313 load of the dye, time duration and pH plays dictating role in the degradation process. The
314 methylene blue showed two characteristic peaks at 292 and 665 nm. A gradual decrease in the
315 absorption intensity was observed in response to the increase in the exposure time [14]. Firstly,
316 degradation of MB by CuFe LDH alone was explored and it was barely 41.56%. In order to
317 enhance its photocatalytic effect; CuFe LDH was doped with RGO and Zr moieties. In this
318 regard, it was noticed that $Zr_{0.4}RGO_{CuFe}$ LDH is relatively less efficient regarding the
319 photodegradation of MB dye compared to $Zr_{0.6}RGO_{CuFe}$ LDH. It degraded 91.5% of MB dye
320 compared to 95.2% of $Zr_{0.6}RGO_{Cu-Fe}$ LDH under similar conditions. Several parameters affect the
321 degradation of MB dye that will be thoroughly discussed in the upcoming sections.

322

323 ***3.2 Effect of pH***

324 The pH is very important parameter which provides insight into the surface and charge properties
325 of the catalyst. The effect of pH was evaluated per catalytic degradation of MB dye as the
326 degradation of dye varied with the change of pH. Figs. 5 and 6 exhibit the degradation efficiency
327 of methylene blue from pH 3.0 to 9.0 under visible light irradiation. It is established that the
328 degradation rate enormously increased from pH 3 to 7.0 and then apparently decreased from 7.0
329 to 9.0. The catalyst showed peak up the degradation efficiency upto 95.2% at pH 7.0 but
330 relatively lower at pH 3.0, 4.5 and 9.5.

331 This performance dwindle was due to leaching of ions from the composite under the influence of
332 harsh acidic conditions. At the basic pH the catalytic efficiency noticed glaring decrease due to
333 the weaker electrostatic force of attraction between negatively charged photocatalyst and the dye
334 [49-51].

335

336

337
338
339
340
341
342
343
344
345
346
347
348
349
350
351
352
353
354
355
356
357
358
359
360

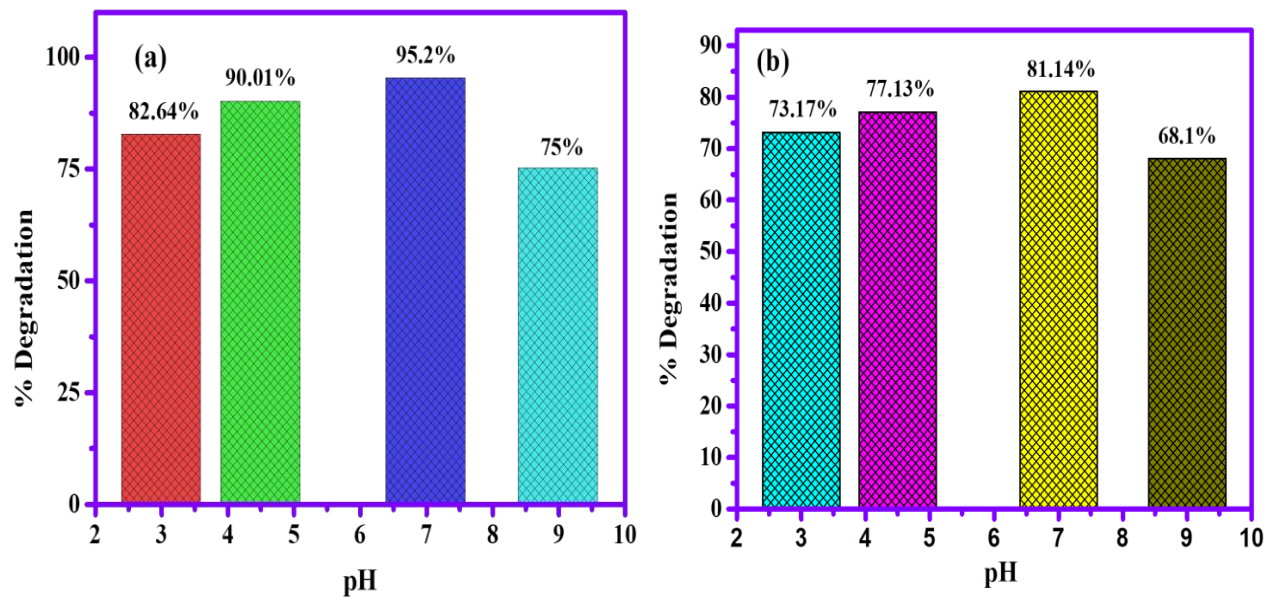


Fig. 5. (a) and (b) Effect of pH on the degradation of MB dye at 10 and 40 ppm dye solutions

3.3 Effect of dye concentration

Two different dye concentrations, 10 and 40 ppm were adopted to evaluate the degradation efficiency. It was discovered that the catalyst exhibited superior photodegradation performance at the lower dye concentrations. But at the higher dye concentration, the catalyst became passive and its photocatalytic potential decreased. It was due to diminishing transparency of waste water; consequently the light will not penetrate the solution to interact with the photocatalyst. Moreover, dye molecules accumulated on the surface of the photocatalyst resulting in the lower catalytic efficiency. Therefore, the degradation performance decreased on increasing concentration of solution from 10 to 40 ppm as depicted in Fig. 6(a-d) and 7(a-d).

361
362
363
364
365
366
367
368
369
370
371
372
373
374
375
376
377
378
379
380
381
382
383
384
385
386
387

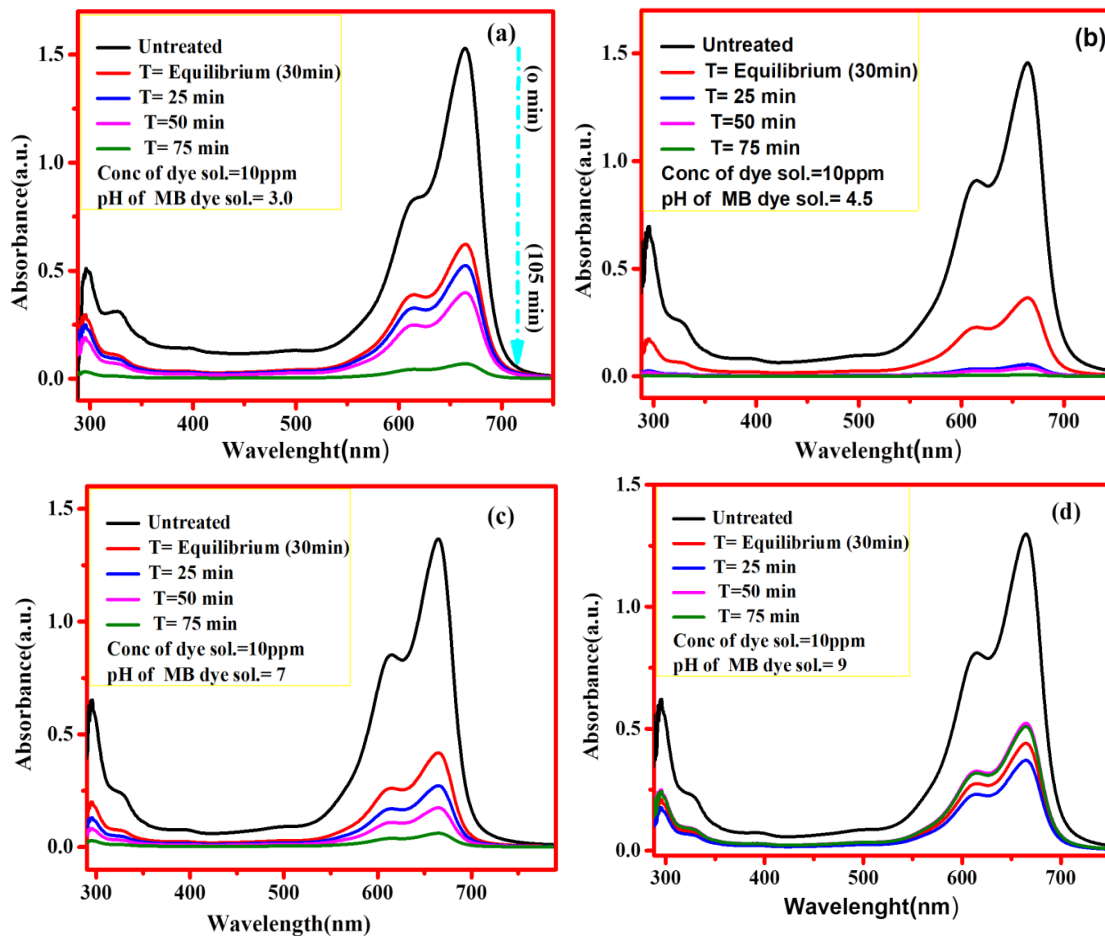


Fig. 6. (a-d) Photodegradation of 10 ppm MB dye at different tested parameters (pH and illumination time)

3.4 Effect of illumination time on dye degradation

The effect of illumination time on the degradation of MB dye appeared in Fig. 6 and 7. This in turn showed that an increase of illumination time from zero to 75 minutes would increase the degradation percentage of methylene blue dye using $Zr_{0.6}S\text{RGOCuFe}$ LDH composite. This can be attributed to activation of the photocatalyst by the absorbing the light radiations. Moreover, no noticeable photodegradation of dye was observed beyond the aforementioned time.

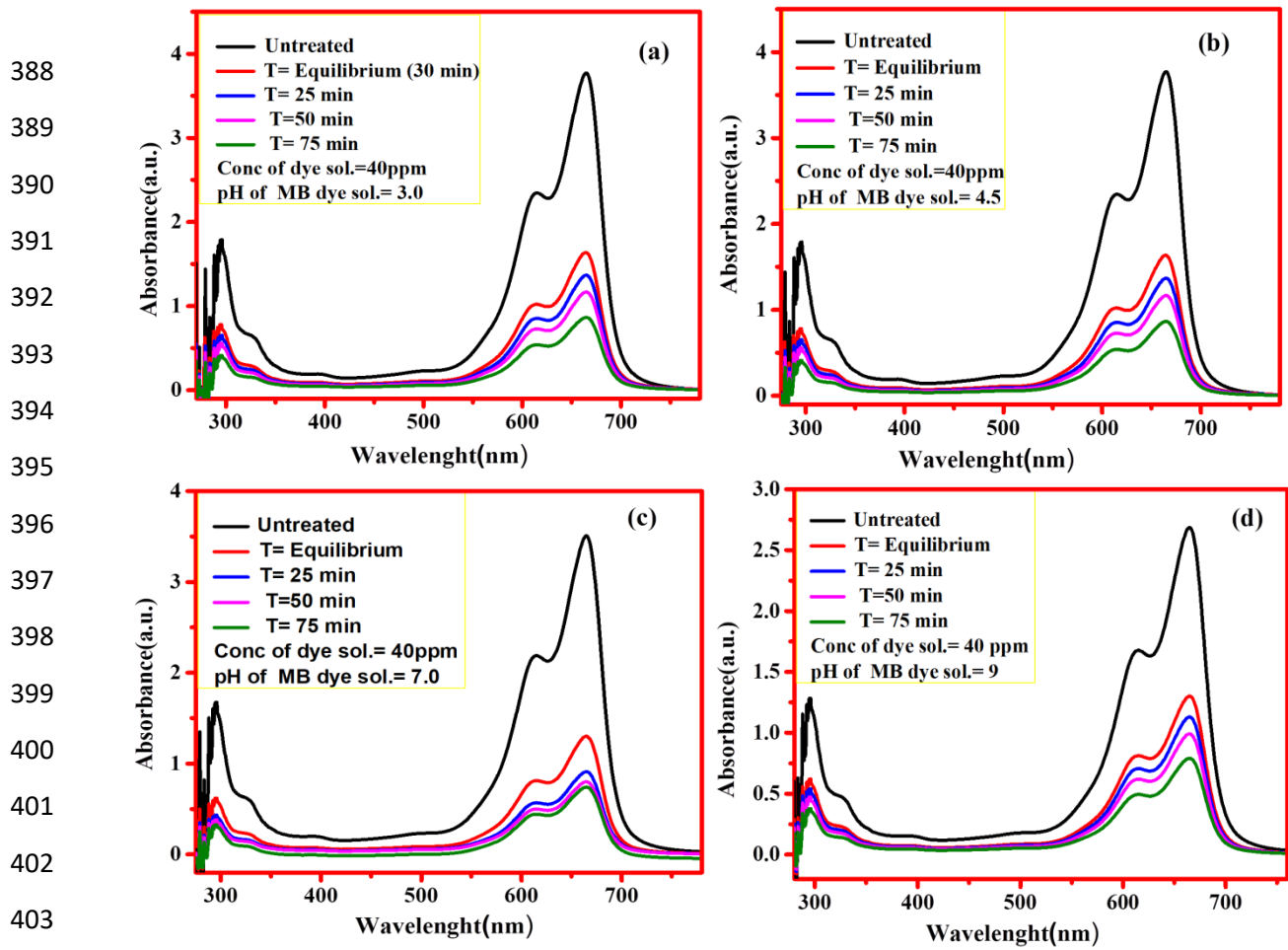


Fig. 7. (a-d) Photodegradation of 40 ppm MB dye at different tested parameters (pH and illumination time)

Table 1 Comparison of degradation performance of Z RGCu-Fe LDH composite and cited literature

Photocatalyst	Light source	TC Concentration (ppm)	Degradation time/ Efficiency	k (min^{-1})	Reference
Ag/Ag ₂ O/BiNbO ₄	LED(84W)	1	240 min/ 84%	0.0061	[52]
2Bi/CN	LED(18W)	10	60 min/ 92%	0.040	[53]
Zn _{0.98} Mn _{0.02} O	UV(8W, C) (Hg-lamp)	10	120 min/ 99%	0.030	[36]
0.2CdS/Mg-Al	Visible radiation	10	90 min/ 94.78%	0.01168	[14]
ND/ LDH	UV(500W Xe lamp)	10	120 min/ 93.5%	0.0233	[54]
Zr _{0.6} RGOCuFe LDH	Visible (200W bulb)	10	75 min/ 95.2%	0.044862	This work

409 From [Table 1](#) it is evident that the degradation results of Zr_{0.6}RGOCuFe LDH are comparable to
410 reported results for the degradation of MB dye but its superiority lies in its lower degradation
411 time span and higher rate constant value (0.044862 min⁻¹). Furthermore, ZrRGOCuFe LDHs
412 composite are visible light active materials as compared to majority of reported photocatalysts
413 requiring UV radiation source or any chemical agents for improving photocatalytic performance
414 of the catalysts.

415 **3.5. Kinetic studies**

416 The first order study for the removal of methylene blue dye was performed under varying
417 conditions of pH and dye concentration. It has been revealed the degradation of organic
418 pollutants such as dyes obey first order kinetics; conveniently pseudo first is augmented to fit
419 experimental data of MB dye. Hence, Langmuir-Hinshelwood model is employed for the
420 determination of rate and kinetics of dye degradation by using equation (4) [55].

$$421 \ln C_t/C_o = -kt \quad (4)$$

422 Where, C_t denotes the concentration of dye solution at a specific time interval, C_o is the initial
423 concentration and k is the pseudo first order rate constant minute⁻¹. Table 2 presents the kinetic
424 parameters related to the isotherms explored at different pH values and dye concentrations. It
425 was noticed that correlation coefficient (R²) values range between 0.94725 and 0.99978 for the
426 first order kinetics of MB degradation. These values indicated the importance of Langmuir-
427 Hinshelwood model to explain first order kinetics for the degradation of MB dye; further [Fig. 8](#)
428 (a and b) supported the suitability of pseudo first order kinetics to explain degradation of dye.

429
430
431

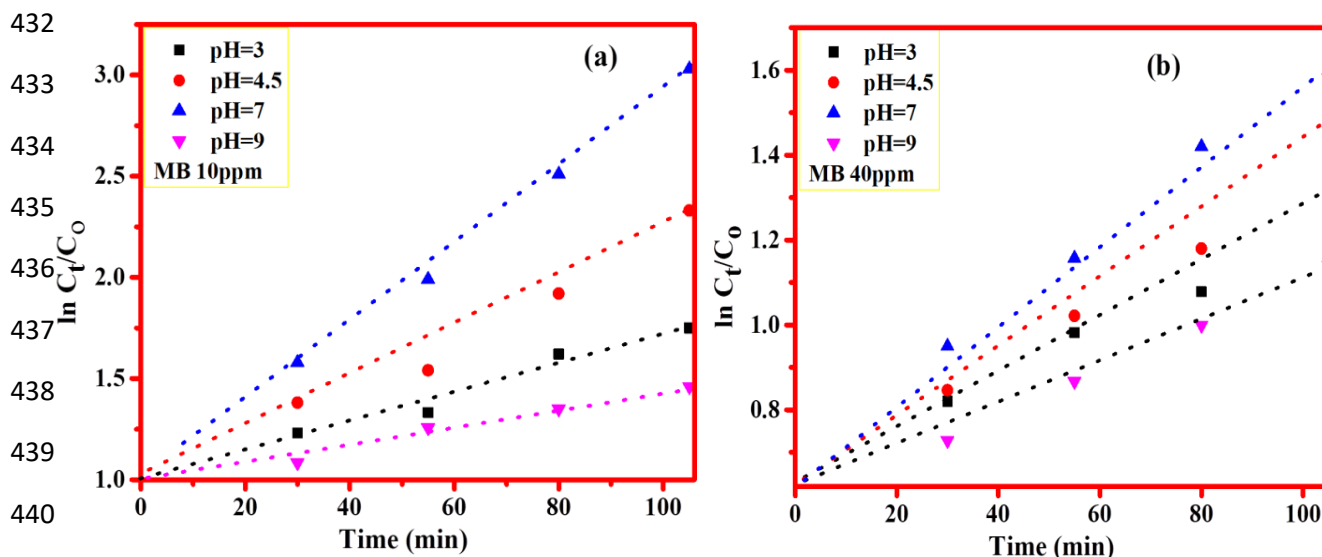


Fig. 8. (a) and (b) Pseudo first order kinetics of dye solution

Table 2 Results of first order kinetic of methylene blue dye degradation

Photocatalyst (g/L)	C_0 (MB) ppm	Initial pH	Pseudo first order $k(\text{min}^{-1})$	R^2
1.0	10	3	0.017042	0.94725
1.0	10	4.5	0.029755	0.9515
1.0	10	7	0.044862	0.99542
1.0	10	9	0.011285	0.97126
1.0	40	3	0.014601	0.95808
1.0	40	4.5	0.018931	0.96533
1.0	40	7	0.020382	0.993
1.0	40	9	0.01262	0.99978

3.6 Reusability of the photocatalyst

The catalytic deactivation was attributed to deposition of carbonaceous materials on the active sites of the photocatalyst and partial leaching of active metals from the surface into the reaction mixture. The used catalyst was centrifuged, separated and then washed with absolute

450 alcohol and deionized several times, finally dried in an oven at 120 °C for six hours [56]. The
451 reusability of the catalyst ZrRGOCuFe LDH was tested by repeating the degradation of MB
452 solution three times with used catalyst at a pH of 7.0 with a catalyst dosage of 1.0g /L. A drastic
453 decrease in the photodegradation has been observed from first to third reusability run, efficiency
454 falls from 95.5 to 65.75 % as shown in Fig.9a. Multiple use of catalyst retarded its ability to
455 exhibit splendid catalytic effect corresponding to entangling of the wreckage of dye on the
456 surface of ZrRGOCuFe LDH composite. The conformity of Zr_{0.6}RGOCuFe LDH composite has
457 shown the capacity of being used for multiple times.

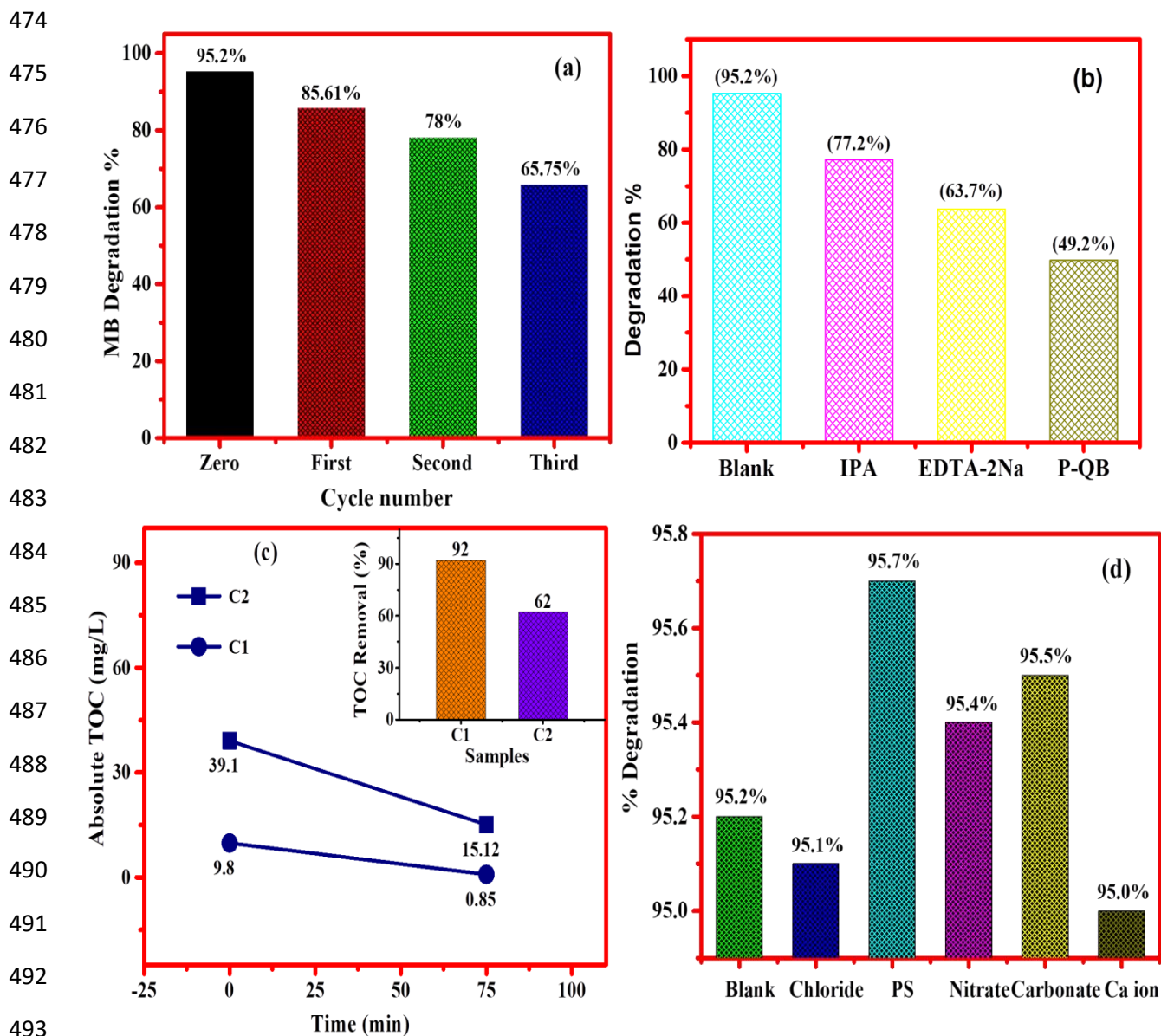
458 **3.7 Stability of the photocatalyst**

459 The stability of the photocatalyst was investigated ZrRGOCuFe LDH for the rea- time
460 application. The doped photocatalyst remained suspended for 2 hours in an aqueous phase which
461 depicts higher dispersion in the water. However, removal efficiency decreased to 87% of the
462 initial 95.2%.

463 **3.7 Determination of total organic content (TOC)**

464 The total carbon analysis was carried out to find mineralization of methylene blue dye. As
465 evident from Fig. 11, the absolute TOC value of the dye C1 (10ppm) decreases from 9.8 to 0.85
466 mg/L with the photomineralization efficiency of 92 % (inset of Fig.9c). However, when the dye
467 concentration is increased C2(40ppm) while retaining the same amount of photocatalyst, the
468 absolute TOC value decreases from 39.1 to 15.12 mg/L photomineralization efficiency is
469 somewhat decreased to 62 % which is attributed to the unavailability of enough active sites on
470 the catalyst surface to carry out the reaction of interest. Moreover, these results also show some
471 leftover TOC in both of these samples which might correspond to the formation of reaction
472 intermediates before they are completely mineralized.

473



494 **Fig. 9.** (a) Reusability of studies of catalyst initial concentration of MB 10 ppm and initial pH 7.0, time 75 minutes
 495 (b) Trapping experiment for the determination mechanism of reaction and effect of species on the adsorption MB
 496 dye (c) Absolute TOC values of different samples of photocatalyst dispersed dye solution at different irradiation
 497 times with respective removal efficiencies (%) in the inset (d) expression for the determination of effect of foreign
 498 ions on the degradation of MB dye.

499 Moreover, these results also show some leftover TOC in both of these samples which might
500 correspond to the formation of reaction intermediates before they are completely mineralized.
501 The demineralization of MB degradation as determined by using following relationship [57],

$$502 \quad \alpha = \frac{\text{TOC}_{\text{init}} - \text{TOC}_{\text{eq}}}{\text{TOC}_{\text{init}}} \times 100 \quad (5)$$

503 Where α represents to the percent mineralization of the MB dye. TOC_{init} and TOC_{eq} describes
504 the initial organic carbon content and equilibrium carbon, respectively.

505 **3.8 Effect of ions and radicals on the adsorption of the of methylene blue dye**

506 The ions and radicals play a substantial role in the degradation of the dyes. The plausible
507 mechanism for the degradation process may be explained based trapping experiments [58]. This
508 aspect may prove useful for the practical degradation of methylene blue dye in the wastewater.
509 Upon irradiation with the suitable light radiations, the photocatalyst may yield three active
510 species such as H⁺ (hole), ·OH (hydroxyl radical), and superoxide (O₂⁻). The species are regarded
511 as essential for the degradation of organic dyes [59]. The trapping activity was performed
512 individually by using different types of scavengers. For this, 1mmol L⁻¹ of EDTA-2Na and
513 isopropanol (IP) solutions were employed as the scavengers of holes (h⁺) and hydroxyl radicals
514 (·OH), respectively. Methylene blue dye solution of 10 ppm and a dye dosage of 1.0 g/L at the
515 pH of 7.0 were specified for the experimentation. A significant suppression in the photocatalytic
516 degradation of MB dye solution was obtained by using different reactive compounds. The
517 suppression in the dye degradation could be ascribed to holes (h⁺) and hydroxyl radicals (·OH),
518 respectively. The effect of peroxide (·O₂⁻) on the degradation of MB dye was investigated by
519 using p-benzoquinone (PBQ). Comparatively, an enhanced suppression in the degradation of MB
520 dye solution was noticed in case of PBQ. Overall, IP, EDTA-2Na and PBQ dye solutions have

521 manifested suppression of 18%, 31.5% and 46% in the degradation of MB, respectively. It has
522 been revealed from the above dye degradation results that holes and hydroxyl radicals promote
523 the photocatalytic degradation of MB dye, while $\cdot\text{O}_2^-$ serves the role of the secondary specie
524 regarding its share in the degradation of dyes. The effect of scavengers on the degradation of MB
525 dye has shown in Fig. 9(b).

526 ***3.9 Effect of foreign ions on the degradation of MB dye***

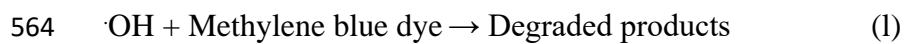
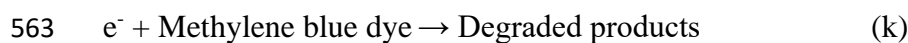
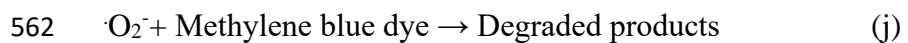
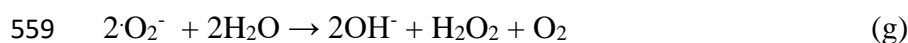
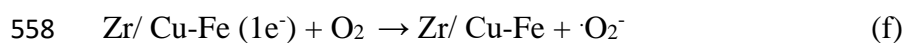
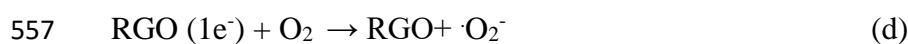
527 The effect of foreign ions on the degradation of MB dye solution was evaluated by using an
528 aqueous solution of 1.0 ml of 10 mM solution of different compounds. The most common
529 interfering species include Cl^- , NO_3^- , $\text{S}_2\text{O}_8^{2-}$ and Ca^{2+} [60]. Methylene blue dye solution of 10
530 ppm and a dye dosage of 1.0 g/L at the pH of 7.0 was stirred for with 1 ml solution of interfering
531 species and stirred for 75 min, followed the same procedure as used for the degradation of dye.
532 The suppression or enhancement effect on the degradation was represented in Fig.9 d. It was
533 revealed that anions promoted the degradation of dye but cations inhibited the degradation
534 process. This study can be applied for the determination of role interfering in the degradation of
535 organic dyes.

536 ***3.11. Proposed mechanism for the dye degradation***

537 Reactive species such as holes (h^+), hydroxyl (OH^\cdot) and superoxide radicals play a notable role
538 in the initiation of photocatalytic degradation of dye. Upon visible light radiation, valence band
539 (VB) electrons get excited and promoted to the conduction band (CB); consequently, a hole was
540 generated in the valence band. Thus reducing molecular oxygen to ($\cdot\text{O}_2^-$) radical, moreover, $\cdot\text{OH}$
541 radical generated by the reaction of hole (h^+) in the valence band by the reaction water [56, 61] .
542 Both RGO and Cu play crucial role as a vital catalytic agent in the composite ZrRGOCuFe LDH.

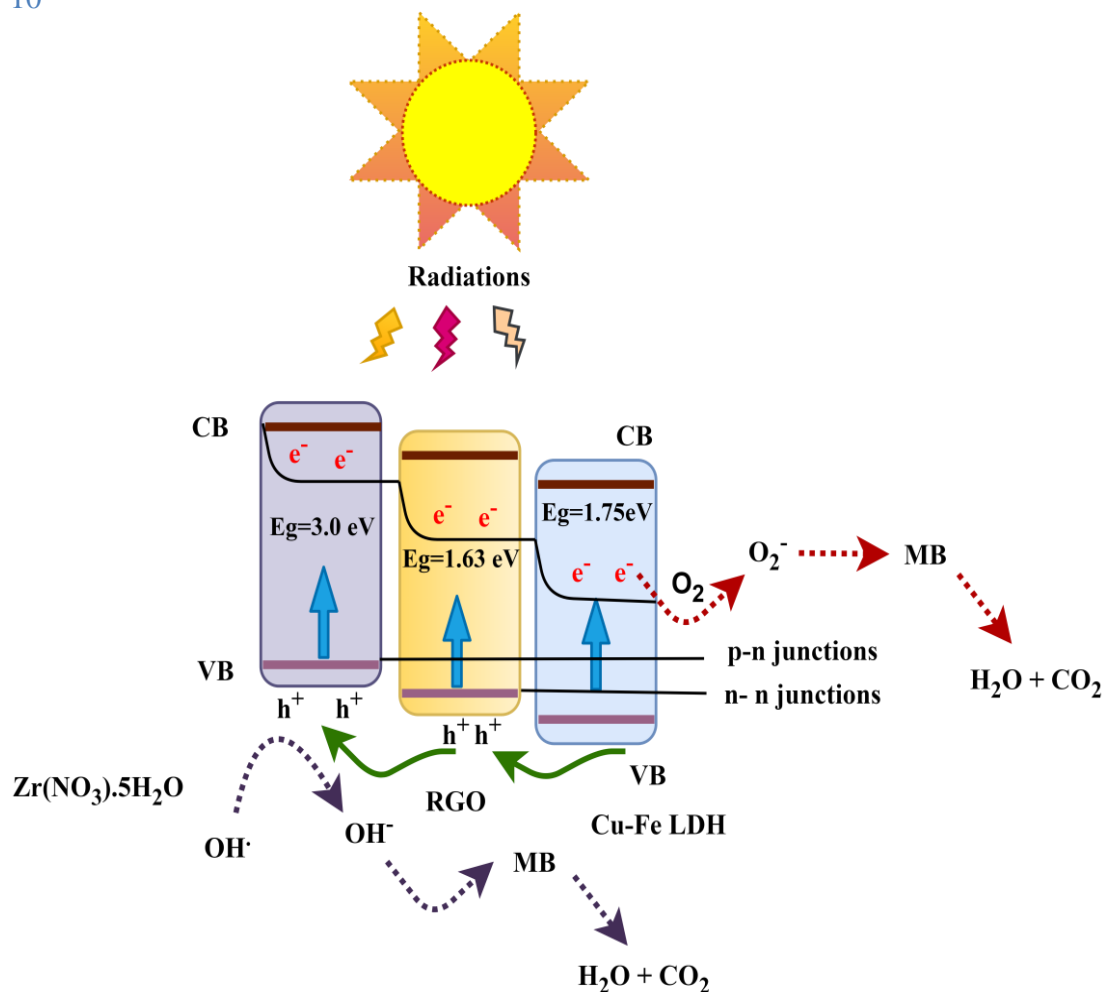
543 Both CuO and RGO may be involved in the production of photo-induced electron and a hole-
544 pair in the presence of visible light radiations. Copper oxide was considered to be the donor of
545 electron while RGO is described as electron acceptor. As per evidence, electron from the
546 conduction band of CuO and Fe₂O₃ in ZrRGO/CuFe LDHs composite moved towards the
547 conduction band of RGO due to its low level. The electron thus obtained from RGO react with
548 O₂ to generate superoxide radicals contrarily holes attacks water or OH to raise ·OH radicals.
549 Moreover, Cu (I) could reduce Fe (III) to Fe (II) [62-66] . In addition to splendid photocatalytic
550 efficiency of RGO and Zr doped CuFe LDH under visible light conditions, these species exhibit
551 efficient degradation of methylene blue. The reaction kinetics of photocatalytic degradation of
552 MB dye is thoroughly presented in the following;

553



565 The photocatalytic mechanism of ZrRGO CuFe LDHs composite is schematically presented in

566 Fig. 10



583 Fig. 10. Proposed mechanism of heterojunction ZrRGO CuFe LDHs composite

584

585 4. Conclusions

586 The heterogeneous photocatalyst ZrRGO CuFe LDHs composite was successfully prepared via

587 facile doping of pristine Cu-Fe by co-precipitation method and its respective products were

588 characterized by FTIR, UV-visible spectroscopy XRD, SEM, EDX, PL, Raman, and EIS. The

589 photodegradation of methylene blue was carried out under varying conditions of dye

590 concentrations such as 10 and 40 ppm, pH 3, 4.5, 7 and 9 while the amount of the photocatalyst

591 was maintained at 1.0 g/L. The precursor Cu-Fe LDH was found to be less effective for the
592 degradation of methylene blue dye solution within 75 min. But $Zr_{0.6}RGO/CuFe$ LDH composite
593 degraded 95.2% of 10 ppm MB dye solution under same conditions. The impressive results of
594 photodegradation revealed that $Zr_{0.6}RGO/CuFe$ LDH composite demonstrated excellent
595 degradation under visible light irradiation and at 25°C. The improved photocatalytic activity was
596 attributed to the synergetic effect between CuFe LDH and RGO which augmented separation and
597 transference of charge. It held relatively good stability and reusability regarding its
598 photodegradation capability even after three successive cycles. The possible degradation method
599 was also explored for the photodegradation by $ZrRGO/CuFe$ LDHs composite. In short,
600 $Zr_{0.6}RGO/CuFe$ LDH composite, the visible light- driven photocatalyst is worth exploring
601 candidate in the practical wastewater.

602 **Declaration of conflict of interest**

603 The authors declare no conflict of interest for this work.

604 **Funding**

605 This research work has been completed with partial help from The Islamia University of
606 Bahawalpur.

607 **Acknowledgement**

608 We would like to thank Materials Chemistry Laboratory and Central Laboratory of the Islamia
609 University of Bahawalpur for the provision of research facilities.

610

611 **References**

612 [1] B. Lellis, C.Z. Fávoro-Polonio, J.A. Pamphile, J.C. Polonio, Effects of textile dyes on health and the
613 environment and bioremediation potential of living organisms, *Biotechnology Research and Innovation*
614 (2019).

615 [2] M.T. Uddin, M.A. Rahman, M. Rukanuzzaman, M.A. Islam, A potential low cost adsorbent for the
616 removal of cationic dyes from aqueous solutions, *Applied Water Science* 7(6) (2017) 2831-2842.

617 [3] N. Atar, A. Olgun, S. Wang, S. Liu, Adsorption of anionic dyes on boron industry waste in single and
618 binary solutions using batch and fixed-bed systems, *Journal of Chemical & Engineering Data* 56(3) (2011)
619 508-516.

620 [4] V. Katheresan, J. Kannedo, S.Y. Lau, Efficiency of various recent wastewater dye removal methods: a
621 review, *Journal of Environmental Chemical Engineering* 6(4) (2018) 4676-4697.

622 [5] S.M. Ahmed, H. Imam, Characterization and photocatalytic activity of Eu: ZnO & Au/Eu: ZnO
623 nanoparticles prepared by laser ablation in water, *Materials Science in Semiconductor Processing* 115
624 (2020) 105128-105138.

625 [6] D. Wróbel, A. Boguta, R.M. Ion, Mixtures of synthetic organic dyes in a photoelectrochemical cell,
626 *Journal of Photochemistry and Photobiology A: Chemistry* 138(1) (2001) 7-22.

627 [7] R.J. Bleicher, D.D. Kloth, D. Robinson, P. Axelrod, Inflammatory cutaneous adverse effects of
628 methylene blue dye injection for lymphatic mapping/sentinel lymphadenectomy, *Journal of surgical*
629 *oncology* 99(6) (2009) 356-360.

630 [8] R.M. Novais, G. Ascensao, D.M. Tobaldi, M.P. Seabra, J.A. Labrincha, Biomass fly ash geopolymer
631 monoliths for effective methylene blue removal from wastewaters, *Journal of Cleaner Production* 171
632 (2018) 783-794.

633 [9] R. Atchudan, T.N.J.I. Edison, S. Perumal, N. Karthik, D. Karthikeyan, M. Shanmugam, Y.R. Lee,
634 Concurrent synthesis of nitrogen-doped carbon dots for cell imaging and ZnO@ nitrogen-doped carbon
635 sheets for photocatalytic degradation of methylene blue, *Journal of Photochemistry and Photobiology A:*
636 *Chemistry* 350 (2018) 75-85.

637 [10] R. Dhanabal, A. Chithambararaj, S. Velmathi, A.C. Bose, Visible light driven degradation of
638 methylene blue dye using Ag₃PO₄, *Journal of environmental chemical engineering* 3(3) (2015) 1872-
639 1881.

640 [11] G. Elango, S.M. Roopan, Efficacy of SnO₂ nanoparticles toward photocatalytic degradation of
641 methylene blue dye, *Journal of Photochemistry and Photobiology B: Biology* 155 (2016) 34-38.

642 [12] M. Mahanthappa, N. Kottam, S. Yellappa, Enhanced photocatalytic degradation of methylene blue
643 dye using CuSCdS nanocomposite under visible light irradiation, *Applied Surface Science* 475 (2019) 828-
644 838.

645 [13] A. Mittal, M. Teotia, R. Soni, J. Mittal, Applications of egg shell and egg shell membrane as
646 adsorbents: a review, *Journal of Molecular Liquids* 223 (2016) 376-387.

647 [14] Z. Li, M. Chen, Z. Ai, L. Wu, Q. Zhang, Mechanochemical synthesis of CdS/MgAl LDH-precursor as
648 improved visible-light driven photocatalyst for organic dye, *Applied Clay Science* 163 (2018) 265-272.

649 [15] S. Ravulapalli, R. Kunta, Effective removal of methylene blue, a hazardous dye from industrial
650 effluents using active carbon of *F. infectoria* plant, *International Journal of Environmental Science and*
651 *Technology* 16(12) (2019) 7837-7848.

652 [16] C. Chen, K. Ruengkajorn, J.-C. Buffet, D. O'Hare, Water adsorbancy of high surface area layered
653 double hydroxides (AMO-LDHs), *RSC advances* 8(60) (2018) 34650-34655.

654 [17] K. Bhuvanewari, G. Palanisamy, T. Pazhanivel, T. Maiyalagan, G. Bharathi, Photodegradation
655 Activity of Nitrogen-rich Graphitic Carbon Nitride Intercalated ZnO\Mg-Al Layered Double Hydroxide
656 Ternary Nanocomposites on Methylene Blue Dye, *ChemistrySelect* 4(11) (2019) 2982-2990.

657 [18] Z. Zhang, Z. Hua, J. Lang, Y. Song, Q. Zhang, Q. Han, H. Fan, M. Gao, X. Li, J. Yang, Eco-friendly
658 nanostructured Zn-Al layered double hydroxide photocatalysts with enhanced photocatalytic activity,
659 *CrystEngComm* 21(31) (2019) 4607-4619.

660 [19] A. Mikhailau, H. Maltanova, S.K. Poznyak, A.N. Salak, M.L. Zheludkevich, K.A. Yasakau, M.G. Ferreira,
661 One-step synthesis and growth mechanism of nitrate intercalated ZnAl LDH conversion coatings on zinc,
662 *Chemical Communications* 55(48) (2019) 6878-6881.

663 [20] X. Fang, Y. Men, F. Wu, Q. Zhao, R. Singh, P. Xiao, T. Du, P.A. Webley, Improved methanol yield and
664 selectivity from CO₂ hydrogenation using a novel Cu-ZnO-ZrO₂ catalyst supported on Mg-Al layered
665 double hydroxide (LDH), *Journal of CO₂ Utilization* 29 (2019) 57-64.

666 [21] M. Djellali, M. Kameche, H. Kebaili, M.M. Bouhent, A. Benhamou, Synthesis of nickel-based layered
667 double hydroxide (LDH) and their adsorption on carbon felt fibres: application as low cost cathode
668 catalyst in microbial fuel cell (MFC), *Environmental Technology* (2019) 1-13.

669 [22] K. Rajendaran, R. Muthuramalingam, S. Ayyadurai, Green synthesis of Ag-Mo/CuO nanoparticles
670 using *Azadirachta indica* leaf extracts to study its solar photocatalytic and antimicrobial activities,
671 *Materials Science in Semiconductor Processing* 91 (2019) 230-238.

672 [23] H. Zhang, M.U. Tahir, X. Yan, X. Liu, X. Su, L. Zhang, Ni-Al layered double hydroxide with regulated
673 interlayer spacing as electrode for aqueous asymmetric supercapacitor, *Chemical Engineering Journal*
674 368 (2019) 905-913.

675 [24] J.B. Joo, Q. Zhang, I. Lee, M. Dahl, F. Zaera, Y. Yin, Mesoporous anatase titania hollow
676 nanostructures through silica-protected calcination, *Advanced Functional Materials* 22(1) (2012) 166-
677 174.

678 [25] L. Mishchenko, B. Hatton, M. Kolle, J. Aizenberg, Patterning hierarchy in direct and inverse opal
679 crystals, *small* 8(12) (2012) 1904-1911.

680 [26] N. Murayama, R. Hara, T. Miyoshi, J. Shibata, E. Udagawa, Synthesis of Layered Double Hydroxide by
681 Co-Precipitation Method from Ca²⁺-Mg²⁺-Al³⁺ Mixed Solution and its Removal Property of Toxic
682 Anions, *Kagaku Kogaku Ronbunshu* 38(4) (2012) 234-241.

683 [27] Z.P. Xu, G.Q. Lu, Hydrothermal synthesis of layered double hydroxides (LDHs) from mixed MgO and
684 Al₂O₃: LDH formation mechanism, *Chemistry of materials* 17(5) (2005) 1055-1062.

685 [28] L. Kong, X. Zhang, C. Wang, F. Wan, L. Li, Synergic effects of Cu_xO electron transfer co-catalyst and
686 valence band edge control over TiO₂ for efficient visible-light photocatalysis, *Chinese Journal of Catalysis*
687 38(12) (2017) 2120-2131.

688 [29] Y. Bu, H. Jang, O. Gwon, S.H. Kim, S.H. Joo, G. Nam, S. Kim, Y. Qin, Q. Zhong, S.K. Kwak, Synergistic
689 interaction of perovskite oxides and N-doped graphene in versatile electrocatalyst, *Journal of materials*
690 *chemistry A* 7(5) (2019) 2048-2054.

691 [30] R. Li, Y. Wang, W. Li, S. Zhou, P. Tian, H. Gao, X. Liu, J. Zang, Ternary NiFeZr layered double
692 hydroxides: a highly efficient catalyst for the oxygen evolution reaction, *Chemical Communications*
693 55(89) (2019) 13370-13373.

694 [31] J. Yan, Y. Chen, L. Qian, W. Gao, D. Ouyang, M. Chen, Heterogeneously catalyzed persulfate with a
695 CuMgFe layered double hydroxide for the degradation of ethylbenzene, *Journal of hazardous materials*
696 338 (2017) 372-380.

697 [32] J. Yan, Y. Chen, W. Gao, Y. Chen, L. Qian, L. Han, M. Chen, Catalysis of hydrogen peroxide with Cu
698 layered double hydroxide for the degradation of ethylbenzene, *Chemosphere* 225 (2019) 157-165.

699 [33] Y. Ma, F. Chen, Q. Yang, Y. Zhong, X. Shu, F. Yao, T. Xie, X. Li, D. Wang, G. Zeng, Sulfate radical
700 induced degradation of Methyl Violet azo dye with CuFe layered double hydroxide as heterogeneous
701 photoactivator of persulfate, *Journal of environmental management* 227 (2018) 406-414.

702 [34] N. Zaaba, K. Foo, U. Hashim, S. Tan, W.-W. Liu, C. Voon, Synthesis of graphene oxide using modified
703 hummers method: solvent influence, *Procedia engineering* 184 (2017) 469-477.

704 [35] Z.-z. Yang, Q.-b. Zheng, H.-x. Qiu, L. Jing, J.-h. Yang, A simple method for the reduction of graphene
705 oxide by sodium borohydride with CaCl₂ as a catalyst, *New Carbon Materials* 30(1) (2015) 41-47.

706 [36] L.A. Chanu, W.J. Singh, K.J. Singh, K.N. Devi, Effect of operational parameters on the photocatalytic
707 degradation of Methylene blue dye solution using manganese doped ZnO nanoparticles, *Results in*
708 *Physics* 12 (2019) 1230-1237.

709 [37] H. Ramezanalizadeh, E. Rafiee, Design, fabrication, electro-and photoelectrochemical investigations
710 of novel CoTiO₃/CuBi₂O₄ heterojunction semiconductor: An efficient photocatalyst for the degradation
711 of DR16 dye, *Materials Science in Semiconductor Processing* 113 (2020) 105055-105066.

712 [38] H. Saleem, M. Haneef, H.Y. Abbasi, Synthesis route of reduced graphene oxide via thermal
713 reduction of chemically exfoliated graphene oxide, *Materials Chemistry and Physics* 204 (2018) 1-7.

714 [39] M. Abbas, Z. Harrache, M. Trari, Removal of gentian violet in aqueous solution by activated carbon
715 equilibrium, kinetics, and thermodynamic study, *Adsorption Science & Technology* (2019) 566-589.

716 [40] Q. Qu, Y. Zhu, X. Gao, Y. Wu, Core-shell structure of polypyrrole grown on V₂O₅ nanoribbon as high
717 performance anode material for supercapacitors, *Adv. Energy Mater.* 2(8) (2012) 950-955.

718 [41] S.S. Imam, Z.U. Zango, H. Abdullahi, Room Temperature Synthesis of Bismuth Oxyiodide with
719 Different Morphologies for the Photocatalytic Degradation of Norfloxacin, *Am. sci. res. j. eng., technol.,*
720 *sci.* 41(1) (2018) 26-39.

721 [42] C.F. Holder, R.E. Schaak, Tutorial on Powder X-ray Diffraction for Characterizing Nanoscale
722 Materials, ACS Publications, 2019, pp. 7359-7365.

723 [43] B. Tong, Z. Deng, B. Xu, G. Meng, J. Shao, H. Liu, T. Dai, X. Shan, W. Dong, S. Wang, Oxygen vacancy
724 defects boosted high performance p-type delafossite CuCrO₂ gas sensors, *ACS applied materials &*
725 *interfaces* 10(40) (2018) 34727-34734.

726 [44] D.P. Sahoo, S. Patnaik, K. Parida, Construction of a Z-Scheme Dictated WO₃-X/Ag/ZnCr LDH
727 Synergistically Visible Light-Induced Photocatalyst towards Tetracycline Degradation and H₂ Evolution,
728 *ACS omega* 4(12) (2019) 14721-14741.

729 [45] H. Prakruthi, B. Chandrashekar, J. Prakash, Y. Bhat, Hydrogenation efficiency of highly porous Cu-Al
730 oxides derived from dealuminated LDH in the conversion of furfural to furfuryl alcohol, *Journal of*
731 *industrial and engineering chemistry* 62 (2018) 96-105.

732 [46] B.M. Pirzada, Pushpendra, R.K. Kunchala, B.S. Naidu, Synthesis of LaFeO₃/Ag₂CO₃ Nanocomposites
733 for Photocatalytic Degradation of Rhodamine B and p-Chlorophenol under Natural Sunlight, *ACS omega*
734 4(2) (2019) 2618-2629.

735 [47] G. Zheng, C. Wu, J. Wang, S. Mo, Z. Zou, B. Zhou, F. Long, Space-Confined Effect One-Pot Synthesis
736 of γ -AlO(OH)/MgAl-LDH Heterostructures with Excellent Adsorption Performance, *Nanoscale research*
737 *letters* 14(1) (2019) 281-293.

738 [48] J. Prithi, N. Rajalakshmi, G.R. Rao, Nitrogen doped mesoporous carbon supported Pt electrocatalyst
739 for oxygen reduction reaction in proton exchange membrane fuel cells, *International Journal of*
740 *Hydrogen Energy* 43(9) (2018) 4716-4725.

741 [49] D.R. Paul, R. Sharma, S. Nehra, A. Sharma, Effect of calcination temperature, pH and catalyst loading
742 on photodegradation efficiency of urea derived graphitic carbon nitride towards methylene blue dye
743 solution, *RSC Advances* 9(27) (2019) 15381-15391.

744 [50] L. Fan, C. Luo, X. Li, F. Lu, H. Qiu, M. Sun, Fabrication of novel magnetic chitosan grafted with
745 graphene oxide to enhance adsorption properties for methyl blue, *J. Hazard. Mater.* 215, (2012) 272-
746 279.

747 [51] Y. Guo, S. Yang, W. Fu, J. Qi, R. Li, Z. Wang, H. Xu, Adsorption of malachite green on micro-and
748 mesoporous rice husk-based active carbon, *Dyes and pigments* 56(3) (2003) 219-229.

749 [52] A. Lebedev, F. Anariba, X. Li, D.S.H. Leng, P. Wu, Ag/Ag₂O/BiNbO₄ structure for simultaneous
750 photocatalytic degradation of mixed cationic and anionic dyes, *Solar Energy* 178 (2019) 257-267.

751 [53] J. Matmin, M.A. Jalani, H. Osman, Q. Omar, N. Ab'lah, K. Elong, M.F. Kasim, Photochemical Synthesis
752 of Nanosheet Tin Di/Sulfide with Sunlight Response on Water Pollutant Degradation, *Nanomaterials* 9(2)
753 (2019) 264-280.

754 [54] L. Liu, S. Li, Y. An, X. Sun, H. Wu, J. Li, X. Chen, H. Li, Hybridization of Nanodiamond and CuFe-LDH as
755 Heterogeneous Photoactivator for Visible-Light Driven Photo-Fenton Reaction: Photocatalytic Activity
756 and Mechanism, *Catalysts* 9(2) (2019) 118-137.

- 757 [55] L.N. Mendez-Alvarado, A. Medina-Ramirez, J. Manriquez, R. Navarro-Mendoza, R. Fuentes-Ramirez,
758 J.M. Peralta-Hernandez, Synthesis of microspherical structures of bismuth oxychloride (BiOCl) towards
759 the degradation of reactive orange 84 dye with sunlight, *Materials Science in Semiconductor Processing*
760 114 (2020) 105086-105095.
- 761 [56] G. Zhao, C. Li, X. Wu, J. Yu, X. Jiang, W. Hu, F. Jiao, Reduced graphene oxide modified NiFe-
762 calcinated layered double hydroxides for enhanced photocatalytic removal of methylene blue, *Applied*
763 *Surface Science* 434 (2018) 251-259.
- 764 [57] A. Ivanets, M. Roshchina, V. Srivastava, V. Prozorovich, T. Dontsova, S. Nahirniak, V. Pankov, A.
765 Hosseini-Bandegharai, H.N. Tran, M. Sillanpää, Effect of metal ions adsorption on the efficiency of
766 methylene blue degradation onto MgFe₂O₄ as Fenton-like catalysts, *Colloids and Surfaces A:*
767 *Physicochemical and Engineering Aspects* 571 (2019) 17-26.
- 768 [58] A. Bhati, S.R. Anand, Gunture, A.K. Garg, P. Khare, S.K. Sonkar, Sunlight-induced photocatalytic
769 degradation of pollutant dye by highly fluorescent red-emitting Mg-N-embedded carbon dots, *ACS*
770 *Sustainable Chemistry & Engineering* 6(7) (2018) 9246-9256.
- 771 [59] A. Singh, P. Khare, S. Verma, A. Bhati, A.K. Sonker, K.M. Tripathi, S.K. Sonkar, Pollutant soot for
772 pollutant dye degradation: soluble graphene nanosheets for visible light induced photodegradation of
773 methylene blue, *ACS Sustainable Chemistry & Engineering* 5(10) (2017) 8860-8869.
- 774 [60] C. Sahoo, A.K. Gupta, I.M. Sasidharan Pillai, Photocatalytic degradation of methylene blue dye from
775 aqueous solution using silver ion-doped TiO₂ and its application to the degradation of real textile
776 wastewater, *Journal of Environmental Science and Health, Part A* 47(10) (2012) 1428-1438.
- 777 [61] B.E. Nagay, C. Dini, J.M. Cordeiro, A.P. Ricomini-Filho, E.D. De Avila, E.C. Rangel, N.C. Da Cruz, V.A.
778 Barão, Visible-Light-Induced Photocatalytic and Antibacterial Activity of TiO₂ Codoped with Nitrogen and
779 Bismuth: New Perspectives to Control Implant-Biofilm-Related Diseases, *ACS applied materials &*
780 *interfaces* 11(20) (2019) 18186-18202.
- 781 [62] A.A. Isari, A. Payan, M. Fattahi, S. Jorfi, B. Kakavandi, Photocatalytic degradation of rhodamine B
782 and real textile wastewater using Fe-doped TiO₂ anchored on reduced graphene oxide (Fe-TiO₂/rGO):
783 Characterization and feasibility, mechanism and pathway studies, *Applied Surface Science* 462 (2018)
784 549-564.
- 785 [63] Y. Ding, L. Zhu, N. Wang, H. Tang, Sulfate radicals induced degradation of tetrabromobisphenol A
786 with nanoscaled magnetic CuFe₂O₄ as a heterogeneous catalyst of peroxymonosulfate, *Applied*
787 *Catalysis B: Environmental* 129 (2013) 153-162.
- 788 [64] J. Zhu, Z. Zhu, H. Zhang, H. Lu, Y. Qiu, Efficient degradation of organic pollutants by
789 peroxymonosulfate activated with MgCuFe-layered double hydroxide, *RSC advances* 9(4) (2019) 2284-
790 2291.
- 791 [65] A. Kumar, G. Sharma, M. Naushad, H. Ala'a, A. Garcia-Penas, G.T. Mola, C. Si, F.J. Stadler, Bio-
792 inspired and biomaterials-based hybrid photocatalysts for environmental detoxification: A review,
793 *Chemical Engineering Journal* 382 (2020) 122937-123019.
- 794 [66] A. Bhati, A. Singh, K.M. Tripathi, S.K. Sonkar, Sunlight-induced photochemical degradation of
795 methylene blue by water-soluble carbon nanorods, *International Journal of Photoenergy* 2016 (2016).

796

797